CRYSTAL GROWTH & DESIGN

Article

pubs.acs.org/crystal

Growth and Optical Properties of Explosion Phase Boron Nitride Octahedron Crystals

Jilin Wang,[†] Yunle Gu,[‡,§] Zili Li,[†] Weimin Wang,*[,†] and Zhengyi Fu[†]

[†]The State Key Laboratory of Advanced Technology for Materials Synthesis and Processing, Wuhan University of Technology, Wuhan 430070, China

[‡]School of Material Science and Engineering, Wuhan Institute of Technology, Wuhan 430073, China

[§]Nano and Ceramic Materials Research Center, Wuhan Institute of Technology, Wuhan 430073, China

ABSTRACT: A low temperature and high pressure synthetic route assisted with ball milling has been established to prepare high quality orientated explosion phase boron nitride (E-BN) octahedron crystals using H_3BO_3, iron powders, NH_4Cl, and Mg as starting materials. FSEM, TEM, HRTEM, SAED, XRD, Raman, FTIR, and XPS were employed for characterization of the morphology and structure of as-synthesized E-BN samples. The E-BN was identified as the face-centered cubic structure with a lattice parameter of 8.245 Å. The typical particle sizes were mainly in the range of 30−120 nm. A UV spectrum indicated that the product has an obvious absorption band (5.61 eV). Photoluminescence spectra revealed that it has a dominant ultraviolet emission peak at 383 nm. The possible chemical reactions as well as the proposed mechanism of the growth of E-BN octahedron crystals were also discussed.

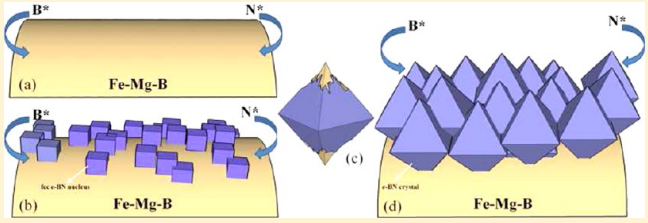

1. INTRODUCTION

The explosion phase boron nitride (E-BN) is a metastable intermediate phase during the transformation between hexagonal BN (h-BN) and cubic BN (c-BN) under high pressures and temperatures, magnetron sputtering, ball milling process, and ion irradiation.[1−5] The new phase was named explosion phase BN (E-BN) owing to its explosion synthetic method.[6] It is considered as a novel phase of BN because of its uniform chemical term but different X-ray diffraction (XRD) pattern, infrared (IR) absorption region, molecular and crystal structures, etc.[7] Previous studies in literature indicate that E-BN revealed some unique properties such as high energy gap, high bulk modulus, low density, and high hardness (even be harder than diamond).[8,9] These unique properties make E-BN an attractive prospect for technological applications in many fields.

Several synthesis techniques have been employed to prepare E-BN, e.g., multiple shock-treatments of h-BN,[10] hydrothermal synthesis,[11] electric- and plasma-assisted chemical vapor deposition,[12,13] supercritical fluid,[8] and electrostatic acceleration methods.[14] However, the major products obtained through these methods were usually E-BN coexisting with other different phases of boron nitride. It is also difficult to obtain pure E-BN samples as bulk solid and thus constrain the further researches on the structures, properties, and applications of E-BN. For instance, Batsanov et al. suggested a rhombic syngony from XRD pattern results with two different parameters.[15,16] Akashi et al. and Nameki et al. identified the prepared E-BN as a face-centered cubic (fcc) symmetry with lattice parameters of 8.405 and 8.313 Å (JCPDF #51-0779), respectively.[17,18] Olszyna et al. first proposed an optimized E-BN fullerence structure of B_9N_9 from the XRD and IR analysis, in which existed equal numbers of sp^2 and sp^3 bonds.[14] After that, Pokropivny et al. demonstrated that E-BN has the diamond-type lattice (a = 10.877 Å) formd with $B_{12}N_{12}$ copopolymerized molecules and suggested to mean "extra-diamond" term instead of "explosion" term in the E-phase name.[19] Therefore, it is urgent to develop an available way to prepare a bulk of E-BN with higher purity and crystalline degree. Only with solving this problem can we carry out the further researches about the structures, properties, and applications of E-BN.

In this article, we report an effective way to grow higher quality orientated explosion phase boron nitride octahedron crystals in an autoclave at a low temperature assisted with ball-milling process. A series of characterizations have been used to verify the fcc structure and lattice parameter of the octahedron E-BN crystals. The possible chemical reactions and proposed mechanism of the growth of the E-BN crystals were discussed. In addition, the optical properties of E-BN crystals were also reported.

2. EXPERIMENTAL SECTION

The raw materials, boric acid (H_3BO_3), reduced iron powder (R-Fe), ammonium chloride (NH_4Cl), and magnesium (Mg) were of analytical pure grade and about 150−300 mesh (50−100 μm) powders. In a typical procedure, 10.22 g of H_3BO_3 and 4.62 g of R-Fe were milled for 10 h by a planet-type ball mill with the revolution and rotation of 500 r/min and 250 r/min, respectively. The obtained milled products were mixed with 18.96 g of NH_4Cl and 2.15 g of Mg

Received: August 29, 2012
Revised: December 12, 2012
Published: December 19, 2012

   dx.doi.org/10.1021/cg3012525 | *Cryst. Growth Des.* 2013, 13, 599−605

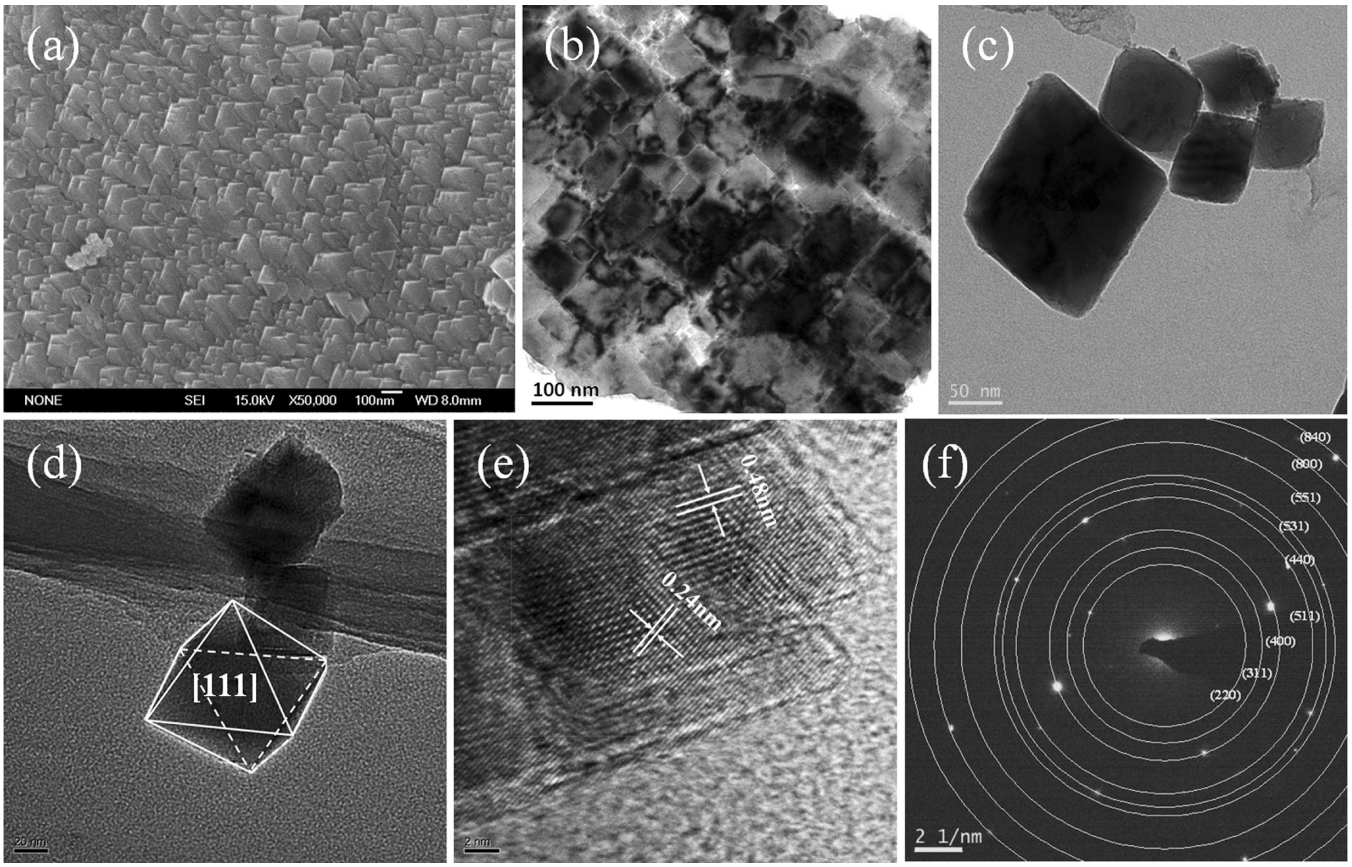

Figure 1. Typical FSEM (a), TEM (b,c,d), and HRTEM (e) images and SAED (f) pattern of the E-BN samples. Scale bars: (a) 100 nm, (b) 100 nm, (c) 50 nm, (d) 20 nm, and (e) 2 nm.

and were put into a 50 mL autoclave. The autoclave was sealed and heated to 550 °C with an increasing speed of 6 °C/min and kept for 6 h in a vertical electric furnace. When the autoclave was cooled to room temperature naturally, it was opened, and the crude product was collected and washed with 5 M hydrochloric acid, ethanol, distilled water, and dried at 80 °C for 24 h. Finally, 3.49 g of E-BN powders were obtained with the yield of about 87.3 wt % based on boron.

The structures of the sample characterized by X-ray powder diffraction (XRD) using Rigaku D/MAX-LLIA X-ray diffractometer with Cu−Kα radiation (wavelength λ = 1.5406 Å). Raman spectrum was recorded at room temperature on a Renishaw Invia Raman spectrometer using an argon-ion laser at excitation of 785 nm. Fourier transform infrared (FTIR) spectra were recorded on a Nicolet Nexus Fourier transform infrared spectrometer using a KBr wafer. Field emission scanning electron microscopy (FSEM) was employed to observe the morphology of the samples using Hitachi S-70 FSEM. The element composition of the sample was determined from the VG Multilab 2000 X-ray photoelectron spectroscopy (XPS) spectra. Transmission electron microscopy (TEM) and high-resolution transmission electron microscopy (HRTEM) were performed on Philips CM12 and JEOL JEM-2100F transmission electron microscopes. UV−vis spectrum was obtained from powders suspended in ethanol using a Shimadzu UV-2550 spectrophotometer.A photoluminescence (PL) spectrum of powders suspended in ethanol was recorded with a 970CRT fluorescence spectrophotometer.

3. RESULTS AND DISCUSSION

3.1. Results. The morphology of the E-BN samples was visualized by FSEM and TEM (Figure 1a−d). The crystals possess a simple octahedron structure with a grain size of 30 to 120 nm. Typical FSEM image (Figure 1a) shows that high-density octahedron structures align fairly closely in the same direction. The corresponding TEM images of the E-BN samples clearly indicate that many single crystals agglomerate together regularly just like building blocks, as shown in Figure 1b. Besides, Figure 1c,d also gives the typical TEM images of the E-BN single crystals. It is obvious that some crystals present translucent three-dimensional octahedron structures, and the complete crystal face [111] could also be observed in Figure 1d.

In order to investigate the inner structural features of the synthesized octahedron E-BN crystals, HRTEM and SAED observations were carried out. The typical HRTEM image (Figure 1e) suggests a well-crystallized structure with the interlayer distances of about 0.48 and 0.24 nm, which corresponds to the (111) and (222) planes of E-BN, respectively, and the two crystal faces with lattice spacing of 0.48 and 0.24 nm in Figure 1e do not belong to the same individual crystal. Meanwhile, the calculated *d*-spacing values forming nine diffraction rings of the corresponding SAED pattern (Figure 1f) are in good agreement with that of (220), (311), (400), (511), (440), (531), (551), (800), and (840) presented in Table 1 and JCPDF card # 51-0779.

The as-synthesized E-BN samples were also characterized by X-ray powder diffraction (XRD), Raman, and Fourier transform infrared (FTIR) spectroscopy. Figure 2a gives the typical XRD pattern of the E-BN samples from 10° to 130°. The observed, calculated *d*-spacing values as well as previous data based on the fcc crystal structure were listed in Table 1. The obtained *d*-spacing values in the range of 10−70° from our work are close to that of the reference data,[18] and the corresponding calculated lattice parameter is a = 8.245 Å, which is slightly lower than the reference values.[17,18] It is worth noting that a weak broad peak

dx.doi.org/10.1021/cg3012525 | *Cryst. Growth Des.* 2013, 13, 599−605

Table 1. XRD and SAED Pattern of the E-BN Sample[a]

hkl	*d*(obs) (nm)	*d*(calcd) (nm)	*d*(ref 17) (nm)	*d*(SAED) (nm)
111	0.4731	0.4760	0.4811	
220	0.2914	0.2915	0.2942	0.2938
311	0.2489	0.2486	0.2506	0.2475
222	0.2380	0.2380	0.2400	
400	0.2063	0.2061	0.2077	0.2071
331	0.1895	0.1892		
422	0.1687	0.1683		
333(511)	0.1592	0.1588	0.1599	0.1609
440	0.1464	0.1458	0.1468	0.1475
531	0.1402	0.1394		0.1404
533	0.1266	0.1257		
444	0.1197	0.1190		
551(711)	0.1161	0.1155		0.1164
642	0.1109	0.1102		
553(731)	0.1082	0.1073		
800	0.1036	0.1031		0.1036
751(555)	0.0961	0.0952		
840	0.0929	0.0922		0.0932
931	0.0872	0.0864		

[a] a_0 = 0.8245 nm; $a_{0(ref)}$ = 0.8313 nm.

located at 2θ = 26.78° also could be observed in the XRD pattern. Its poorly crystallized byproduct hexagonal BN is possibly formed during the temperature preservation stage or resulted from the reversible phase transformation of E-BN during temperature reduction, opening autoclave, and pressure relief processes.[1−6,17,18] In the matter of fact, it is difficult to completely eliminate h-BN in the growth processes of intermediate phase E-BN. However, it is feasible to reduce the content of h-BN as much as possible through controlling the experimental conditions properly such as time, temperature, and raw materials. The Raman (Figure 2b) result demonstrates that the samples are composed of E-BN and h-BN powders.[14] Figure 2c,d shows the typical wide-scan FTIR spectrum in the range of 500 to 4000 cm^{-1} and the corresponding deconvolution spectrum of the E-BN samples, respectively. Seven main peaks located at 403, 512, 642, 792, 1270, 1385, and 1540 cm^{-1} could be observed. Two peaks at 792 and 1385 cm^{-1} are usually attributed to sp^2 chemical bonds of h-BN.[20] Although XRD and Raman analysis indicates that a small amount of byproduct h-BN exists, the corresponding FTIR peaks are very strong. It can be speculated that the two peaks are not entirely due to byproduct h-BN. The other peaks could be ascribed to sp^3 chemical bonds of c-BN. However, the spectrum does not contain the other peaks corresponding to c-BN such as 700, 1830, 2000, and 2230 cm^{-1}.[5,7,21] According to the structure model proposed by Olszyna et al, the E-BN molecule contains equal numbers of sp^3 and sp^2 bonds.[14] In addition, the previous researches also support our results.[7,14,19,22] Therefore, taking the influence of little h-BN into consideration, together with XRD, Raman results, and previous reports, we conclude that the obtained product was E-BN.

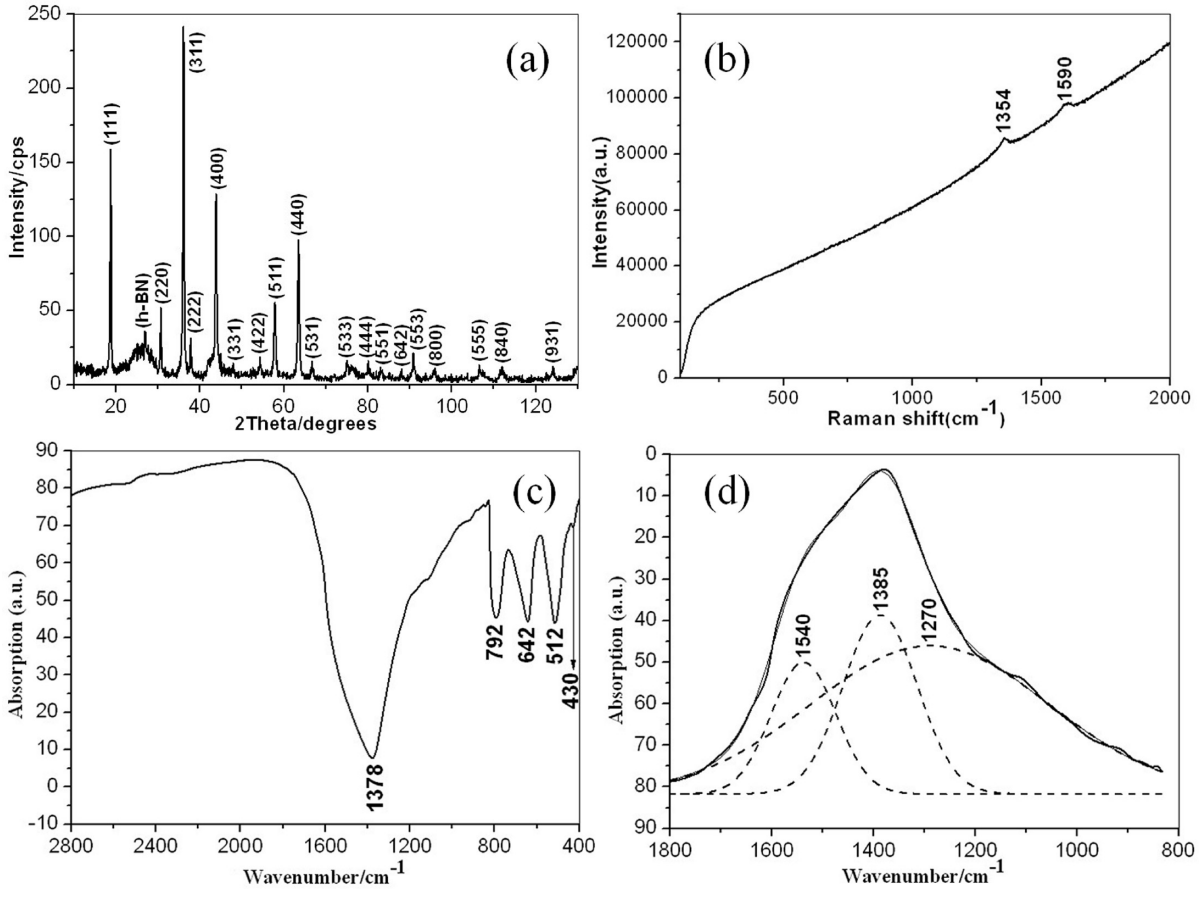

Figure 2. Typical XRD pattern (a), Raman (b), FTIR (c), and deconvolution FTIR (d) spectra of the E-BN samples.

dx.doi.org/10.1021/cg3012525 | *Cryst. Growth Des.* 2013, 13, 599−605

The XPS spectrum of the E-BN samples is shown in Figure 3. Eleven primary peaks located at 47.1, 89.9, 191.6, 285.2, 307.2, 352.9, 399.2, 532.8, 578.5, 589.3, and 978.1 eV could be corresponded to Mg2p, Mg2s, B1s, C1s, Mg(KLL), Mg(KLL), N1s, O1s, Cr2p, Cr2p, and O(KLL), respectively.[23−28] Quantitative analysis of B1s and N1s peaks demonstrates the molar ratio of N/B is 1:1.032, which is close to that of BN.

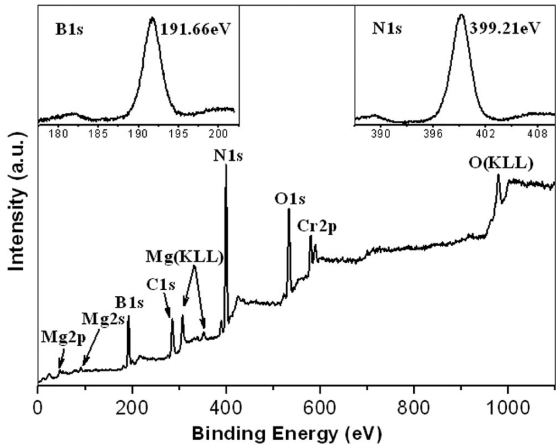

Figure 3. Typical wide scan, B1s (inset, upper left) and N1s (inset, upper right) XPS spectra of the E-BN samples.

In the matter of fact, Pokropivny et al. reported an "extra-diamond" boron nitride (a = 10.877 Å), while Nameki et al. reported another "explosion" boron nitride (a = 8.313 Å). These two materials are different with each other and should have two different definition names. We suggest the sample reported by Pokropivny et al. could use the name "extra-diamond" boron nitride or "extra-diamond BN," and the sample produced in this article could use the name of "explosion" boron nitride or "E-BN" because it displays a very similar structure with that of Nameki et al. In our opinion, because the explosion phase boron nitride (E-BN) is a metastable intermediate phase, which is usually synthesized at high temperature and high pressure, it is reasonable to name this boron nitride according to the first synthetic method before finding a more accurate naming term.

3.2. Chemical Reaction Mechanism. In this experiment, the possible chemical reactions could be described as follows:

$$\mathrm{Fe} + 2\mathrm{H_3BO_3} + 4\mathrm{NH_4Cl} + \mathrm{Mg} = 2\mathrm{BN} + \mathrm{MgCl_2} + \mathrm{FeCl_2} + 2\mathrm{NH_3} + 6\mathrm{H_2O} + 2\mathrm{H_2} \quad (1)$$

$$\mathrm{Fe} + \mathrm{H_3BO_3} \rightarrow [\mathrm{Fe^*{-}B^*{-}O{-}H}] \quad (2)$$

$$2\mathrm{NH_4Cl} \rightarrow 2\mathrm{N^*} + 3\mathrm{H_2} + 2\mathrm{HCl} \quad (3)$$

$$\mathrm{Mg} + [\mathrm{Fe^*{-}B^*{-}O{-}H] \rightarrow [Mg{-}Fe^*{-}B^*]alloy} + \mathrm{MgO} + \mathrm{H_2O} \quad (4)$$

$$\mathrm{N^*} + [\mathrm{Mg{-}Fe^*{-}B^*]alloy} \rightarrow [\mathrm{Mg{-}Fe{-}B^*{-}N^*]alloy} \rightarrow \text{E-BN} + [\mathrm{Mg{-}Fe}] \quad (5)$$

$$[\mathrm{Mg{-}Fe{-}B^*{-}N^*]alloy} \rightarrow \text{E-BN} + [\mathrm{Mg{-}Fe}] \quad (6)$$

$$6\mathrm{HCl} + \mathrm{MgO} + [\mathrm{Mg{-}Fe}] \rightarrow 2\mathrm{MgCl_2} + \mathrm{FeCl_2} + 2\mathrm{H_2} + \mathrm{H_2O} \quad (7)$$

E-BN powders were synthesized according to the reaction described in eq 1. The Gibbs energies for reactions 1, 3, 4, and 7 were calculated as −67.24, −46.14, −6.01, and −14.32 kJ/mol at 600 °C, respectively. The negative values indicate the rationality of the proposed reactions. First, active [Fe*−B*−O−H] could be produced after ball-milling process (eq 2). Second, during the starting growth process, NH_4Cl was decomposed to chemically active N* atoms and H_2 gas (eq 3).[29,30] Third, [Fe*−B*−O−H] was reduced by Mg and generated [Mg−Fe*−B*] alloy, MgO, and H_2O gas (eq 4). According to the catalytic VLS growth mechanism,[31] E-BN may nucleate and grow on the surface of the [Mg−Fe−B*−N*] alloy with the assistance of in situ formed liquid catalyst [Mg−Fe] (eqs 5 and 6).[32] Finally, the catalyst [Mg−Fe] and byproduct MgO reacted with HCl and produced $MgCl_2$, $FeCl_2$, H_2, and H_2O (eq 7).

3.3. Growth Mechanism. Figure 4 illustrates a proposed growth model for octahedron E-BN crystals. Figure 5 shows the FSEM and TEM images of the E-BN samples under different reaction conditions. First, [Mg−Fe*−B*] liquid drop was prepared through the reduction reaction between Mg and [Fe*−B*−O−H] (Figure 4a). Second, many fcc E-BN nuclei with different particle sizes formed on the surface of [Mg−Fe*−B*] liquid drop when the chemical active B* and N* species were supersaturated (Figure 4b). Third, with the

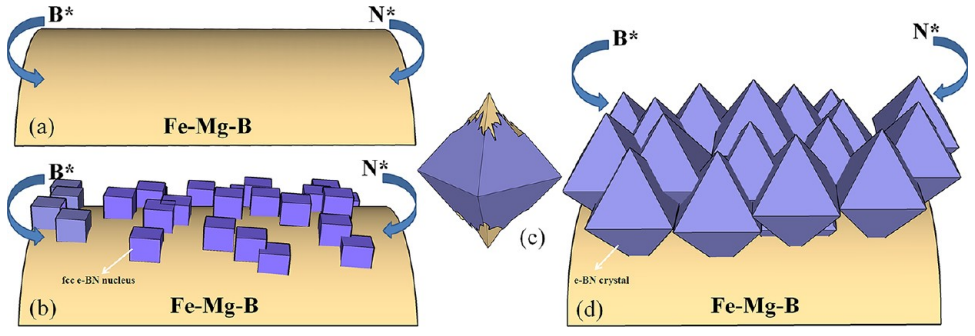

Figure 4. Schematic illustration of the growth models of the E-BN samples. (a) Original [Mg−Fe−B] liquid drop; (b) E-BN nuclei formed on the surface of [Mg−Fe−B] liquid drop; (c) growing octahedron E-BN crystal; (d) orientated growth of octahedron E-BN crystals.

dx.doi.org/10.1021/cg3012525 | Cryst. Growth Des. 2013, 13, 599−605

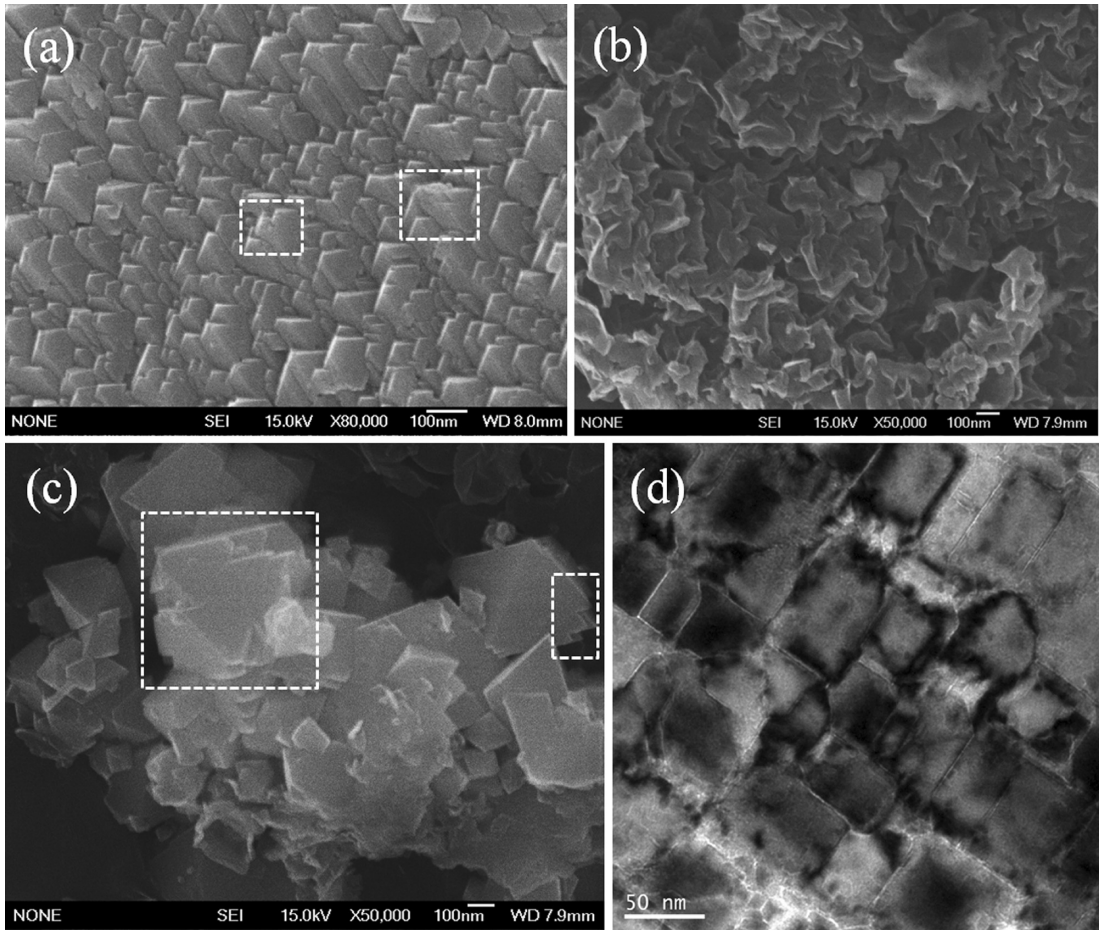

Figure 5. Typical FSEM (a,c) and TEM (d) images of the E-BN samples. (b) Typical FSEM image of lamellar h-BN. Scale bars: (a) 100 nm, (b) 100 nm, (c) 100 nm, and (d) 50 nm.

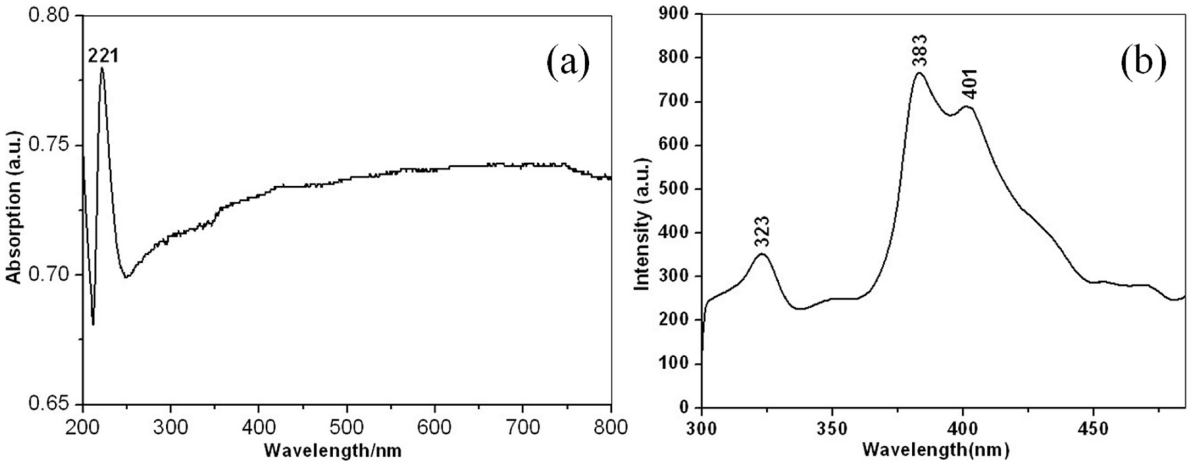

Figure 6. Typical UV−vis absorption spectrum (a) and PL spectrum (b) of the E-BN samples.

continuous supply of B* and N* under a high atmospheric pressure, the directions of [100] and [111] faces preferentially grow to satisfy the geometric criterion of a low energy.[33] During the growth process, the B* and N* atoms precipitate slowly layer by layer on the crystal face [100] and [111] (Figure 4c). In addition, because the [100] face has a higher energy than that of [111], the growth rate of [100] is lower than that of [111].[33] These phenomena could also be confirmed through the observed morphology of the octahedron E-BN crystals in Figure 5a,c (pointed with white frames). Finally, octahedron E-BN crystals were prepared on the catalyst alloy liquid drop (Figure 4d and Figure 5d). The growth of octahedron E-BN will not be terminated unless the B or N atoms are consumed. Moreover, maybe a few octahedron E-BN crystals grew imperfectly when the growth processes stopped. It could be shown in SEM images (pointed with white frames in Figure 5a,c) and the proposed model in Figure 4c.

dx.doi.org/10.1021/cg3012525 | *Cryst. Growth Des.* 2013, 13, 599−605

$$Fe + 2H_3BO_3 + 4NH_4Cl + Mg = 2BN + MgCl_2 + FeCl_2 + 2NH_3 + 6H_2O + 2H_2 \quad (8)$$

In addition, the existence of catalyst R-Fe is essential for preparing a large amount of high quality octahedron E-BN crystals. The Gibbs energy of the reaction without R-Fe (eq 8) was calculated as −60.93 kJ/mol at 600 °C, which is higher than that of the reaction containing catalyst R-Fe (eq 1, −67.24 kJ/mol). Further, one FSEM image suggests that the reactants without R-Fe will lead to almost lamellar h-BN (Figure 5b). It implies that the added catalyst R-Fe will improve the growth of octahedron E-BN crystals. The theoretical calculation was in good agreement with the obtained experiment result.

3.4. UV−visible (UV−vis) and Photoluminescence (PL) Properties. Figure 6a presents the UV−vis absorption spectrum of the E-BN samples. One intense absorption band is centered at 221 nm (5.61 eV), which was different from that of single crystal c-BN (6.1−6.4 eV) and h-BN (5.7−6.0 eV).[34−39] Besides, PL emission spectroscopy was also employed to characterize the E-BN samples by excitation with a laser line at 254 nm. The PL spectrum (Figure 6b) was dominated by a band centered at 383 nm (3.24 eV), and two other less intensive bands appear at 323 nm (3.84 eV) and 401 nm (3.09 eV), which was different from that of c-BN (2.4−2.6 eV) and h-BN (3.4−3.8 eV).[40−43] Actually, these optical results may be influenced by the morphology, structure, residual impurities, and intrinsic defect of E-BN samples, such as band-to-band optical transition and B or N vacancies.[39] These optical properties of octahedron E-BN crystals will be the prerequisite of the potential applications in the fields of ultraviolet optoelectronics devices and ultraviolet lasers.[36,39]

4. CONCLUSIONS

In summary, higher quality orientated growth of octahedron E-BN crystals was successfully synthesized through a low temperature approach assisted with ball-milling process. The characterization results show that the E-BN presents a fcc structure with a lattice parameter of a = 8.245 Å. The contrast experiment indicates that R-Fe plays a significant role in the growth of higher quality octahedron E-BN crystals. A chemical reaction mechanism and VLS growth model of E-BN were proposed. We hope this work is helpful for the further research on the structure, property, and application of E-BN.

AUTHOR INFORMATION

Corresponding Author

*Tel/Fax: +86 27 87215421. E-mail: wangwm@hotmail.com.

Notes

The authors declare no competing financial interest.

ACKNOWLEDGMENTS

We acknowledge the financial support from the National Science Foundation of China (A3 Foresight Project No. 51161140399), the Fundamental Research Funds for the Central Universities (No. 123201003), and the New Century High-level Personnel Project of Hubei Province.

REFERENCES

(1) He, L.; Akaishi, M.; Horiuchi, S. *Microsc. Res. Tech.* **1998**, *40*, 243−250.
(2) Yang, X.; Li, H.; Li, Y.; Lu, X.; Gao, S.; Zhu, P.; Zhang, Q.; Zhang, T.; Zou, G. *J. Cryst. Growth* **2009**, *311*, 3716−3720.
(3) Gasgnier, M.; Szwarc, H.; Ronez, A. *J. Mater. Sci.* **2000**, *35*, 3003−3009.
(4) Zdunek, K.; Sokolowska, A.; Elkaseh, A. *Diamond Relat. Mater.* **1995**, *4*, 381−385.
(5) Mirkarimi, P. B.; McCarty, K. F.; Medlin, D. L. *Mater. Sci. Eng. R* **1997**, *21*, 47−100.
(6) Batsanov, S. S.; Blokhina, C. E.; Deribas, A. A. *J. Struct. Chem.* **1965**, *6*, 209−213.
(7) Wang, J. B.; Zhong, X. L.; Zhang, C. Y.; Huang, B. Q.; Yang, G. W. *J. Mater. Res.* **2003**, *18*, 2774−2778.
(8) Batsanov, S. S. *Diamond Relat. Mater.* **2011**, *20*, 660−664.
(9) Pokropivny, V. V.; Smolyar, A. S.; Pokropivny, A. V. *Phys. Solid State* **2007**, *49*, 591−598.
(10) Akashi, T.; Sawaoka, A.; Saito, S.; Araki, M. *Jpn. J. Appl. Phys.* **1976**, *15*, 891−892.
(11) Hao, X.; Dong, S.; Fang, W.; Zhan, J.; Li, L.; Xu, X.; Jiang, M. *Inorg. Chem. Commun.* **2004**, *7*, 592−594.
(12) Olszyna, A.; Kowalski, B.; Szmidt, J. *Diamond Relat. Mater.* **1994**, *3*, 840−843.
(13) Olszyna, A.; Muftah, M.; Sokolowska, A. *Diamond Relat. Mater.* **1995**, *4*, 386−389.
(14) Olszyna, A.; Konwerska-Hrabowska, J.; Lisicki, M. *Diamond Relat. Mater.* **1997**, *6*, 617−620.
(15) Batsanov, S. S.; Kopaneva, L. I.; Lazareva, E. V.; Kulikova, I. M.; Barinsky, R. L. *Propellants Explos. Pyrotech.* **1993**, *18*, 352−355.
(16) Batsanov, S. S. *Russ. J. Inorg. Chem.* **1983**, *28*, 1545−1550.
(17) Akashi, T.; Pak, H.; Sawaoka, A. B. *J. Mater. Sci.* **1986**, *21*, 4060−4066.
(18) Nameki, H.; Sekine, T.; Kobayashi, T.; Fat'yanov, O. V.; Sato, T.; Tashiro, S. J. *Mater. Sci. Lett.* **1996**, *15*, 1492−1494.
(19) Pokropivny, A. V. *Diamond Relat. Mater.* **2006**, *15*, 1492−1495.
(20) Lee, C. H.; Xie, M.; Kayastha, V.; Wang, J. S.; Yap, Y. K. *Chem. Mater.* **2010**, *22*, 1782−1787.
(21) Gielisse, P. J.; Mitra, S. S.; Pendl, J. N.; Griffis, R. D.; Mansur, L. C.; Marshall, R.; Pascoe, E. A. *Phys. Rev.* **1967**, *155*, 1039−1046.
(22) Guo, J.; Wang, H.; Zhu, J.; Zheng, K.; Zhu, M.; Yan, H.; Yoshimura, M. *Electrochem. Commun.* **2007**, *9*, 1824−1827.
(23) Panayiotatos, Y.; Logothetidis, S.; Handrea, M.; Kautek, W. *Diamond Relat. Mater.* **2003**, *12*, 1151−1156.
(24) Rammanauskas, R.; Gudaviciute, L.; Diaz-Ballote, L.; Bartolo-Perezb, P.; Quintana, P. *Surf. Coat. Technol.* **2001**, *140*, 109−115.
(25) Long, Z. L.; Zhou, Y. C.; Xiao, L. *Appl. Surf. Sci.* **2003**, *218*, 123−136.
(26) Zhang, X.; Van den Bos, C.; Sloof, W. G.; Hovestad, A.; Terrync, H.; de Wit, J. H. W. *Surf. Coat. Technol.* **2005**, *199*, 92−104.
(27) Yu, G. H.; Peng, X. *Appl. Surf. Sci.* **2010**, *256*, 6592−6595.
(28) Shan, L.; Zhang, X. *J. Rare Earths* **2006**, *24*, 310−313.
(29) Dai, J.; Xu, L.; Fang, Z.; Sheng, D.; Guo, Q.; Ren, Z.; Wang, K.; Qian, Y. *Chem. Phys. Lett.* **2007**, *440*, 253−258.
(30) Qian, Q.; Wang, J.; Gu, Y.; Li, J.; Zhao, G.; Zhang, L.; Pan, X. *Mater. Lett.* **2011**, *65*, 866−868.
(31) Wagner, R. S.; Ellis, W. C. *Appl. Phys. Lett.* **1964**, *4*, 89−90.
(32) Wang, J.; Zhang, L.; Zhao, G.; Gu, Y.; Zhang, Z.; Zhang, F.; Wang, W. *J. Solid State Chem.* **2011**, *184*, 2478−2484.
(33) Wang, N.; Cao, X.; Guo, L.; Yang, S.; Wu, Z. *ACS Nano* **2008**, *2*, 184−190.
(34) Soltani, A.; Barkad, H. A.; Mattalah, M.; Benbakhti, B.; De Jaeger, J. C.; Chong, Y. M.; Zou, Y. S.; Zhang, W. J.; Lee, S. T.; BenMoussa, A.; Giordanengo, B.; Hochedez, J. F. *Appl. Phys. Lett.* **2008**, *92*, 053501−053503.
(35) Remes, Z.; Nesladek, M.; Haenen, K.; Watanabe, K.; Taniguchi, T. *Phys. Status Solidi A* **2005**, *202*, 2229−2233.
(36) Kubota, Y.; Watanabe, K.; Tsuda, O.; Taniguchi, T. *Science* **2007**, *317*, 932−934.
(37) Watanabe, K.; Taniguchi, T.; Kanda, H. *Phys. Status Solidi A* **2004**, *201*, 2561−2565.

(38) Zhi, C.; Bando, Y.; Tang, C.; Xie, R.; Sekiguchi, T.; Golberg, D. *J. Am. Chem. Soc.* **2005**, *127*, 15996−15997.
(39) Zhi, C.; Bando, Y.; Tang, C.; Golberg, D.; Xie, R.; Sekiguchi, T. *Appl. Phys. Lett.* **2005**, *92*, 213110−213113.
(40) Trinkler, L.; Berzina, B.; Benabdesselam, M.; Iacconi, P.; Bøtter-Jensenc, L.; Atobe, K. *Radiat. Meas.* **2004**, *38*, 615−618.
(41) Berzina, B.; Trinkler, L.; Atobe, K. *Phys. Status Solidi C* **2002**, *1*, 421−424.
(42) Oku, T.; Hirano, T.; Kuno, M.; Kusunose, T.; Niihara, K.; Suganuma, K. *Mater. Sci. Eng., B* **2000**, *74*, 206−217.
(43) Wu, J.; Han, W.; Walukiewicz, W.; AgerIII, J.; Shan, W.; Haller, E.; Zettl, A. *Nano Lett.* **2004**, *4*, 647−650.